Extended Finite Element Method Enhanced by Exact Boundary Representation for Analysis of Eddy Currents

Shingo Hiruma

Graduate School of Engineering, Kyoto University, Kyoto, Japan, hiruma.shingo.3w@kyoto-u.ac.jp

The extended finite element method (XFEM) is utilized for high-frequency eddy current analysis. However, when a conductor with a curved surface is involved, the geometric approximation tends to degrade due to the coarse mesh used in XFEM. To enhance the approximation accuracy, exact boundary representation methods are employed within XFEM for eddy current analysis. The proposed method is validated using a round conductor model, demonstrating a substantial reduction of error in global quantities such as Joule losses compared to conventional methods.

***Index Terms*—Eddy currents, isogeometric analysis, isparametric FEM, NURBs-enhanced FEM, p-FEM, XFEM**

I. Introduction

As the switching frequency increases, it becomes more important to evaluate eddy current losses in electromagnetic devices. However, the use of the conventional finite element method (FEM) can be limiting in the computation of the eddy currents at high frequencies because the fine discretization in the conductive domain is required to capture the localized current density near the conductor surface, known as the skin effect. Typically, the size of the finite element must be smaller than the skin depth, which is usually significantly smaller than the size of the electromagnetic devices. Consequently, a considerable amount of computational resources is required as the frequency becomes higher.

To address these challenges, various approaches have been proposed to reduce the computational cost of the eddy current analysis while maintaining acceptable accuracy such as the surface impedance boundary condition (SIBC) [1][2], homogenization methods [3][4], and model order reduction (MOR) methods [5]. Each method has its strengths and weaknesses. For example, SIBC is accurate at high frequencies but inaccurate at low frequencies. The homogenization method is good at modeling the microstructure of materials but is difficult to apply to a complex structure of conductors. The MOR methods can significantly reduce the size of the equation, but we should take the skin depth into account when generating the mesh.

Recently, the author proposed a method using the extended FEM (XFEM) [6] for the eddy current analysis. In XFEM, we can use the coarse mesh for the eddy current analysis with no concern for the skin depth at high frequencies. However, the use of coarse meshes introduces errors resulting from geometric approximation. To overcome this limitation, the proposed method combines XFEM with exact boundary representation (EBR) methods such as isoparametric FEM [7], p-FEM [7], NURBs-enhanced FEM (NEFEM) [8], and isogeometric analysis (IGA) [9]. The effectiveness of the proposed XFEM with EBR is demonstrated through applications in skin and proximity effect analyses, showing a reduction in the number of unknowns compared to conventional FEM (CFEM) and improving accuracy with almost the same memory consumption and computation time as XFEM without EBR.

Manuscript received April 1, 2015; revised May 15, 2015 and June 1, 2015; accepted July 1, 2015. Date of publication July 10, 2015; date of current version July 31, 2015. (Dates will be inserted by IEEE; “published” is the date the accepted preprint is posted on IEEE Xplore®; “current version” is the date the typeset version is posted on Xplore®). Corresponding author: S. Hiruma (e-mail: hiruma.shingo.3w@kyoto-u.ac.jp).

Color versions of one or more of the figures in this paper are available online at http://ieeexplore.ieee.org.

Digital Object Identifier (inserted by IEEE).

II. Proposed method

A. Extended finite element method for eddy current analysis

XFEM is the extended version of FEM, which can be used to model discontinuities, holes, and crack tips. These features are typically challenging to consider in CFEM due to the discontinuity or singularity of the field values [10]. To incorporate prior knowledge about these features, enrichment functions are introduced to expand the solution space. This framework can be applied to a wide variety of problems by designing the enrichment functions appropriately [11].

In the eddy current analysis, the author has proposed to use the exponential function as the enrichment function:

$$\psi(\boldsymbol{x}) = \exp\big(-\gamma d(\boldsymbol{x})\big) \tag{1}$$

where $\gamma = (1+j)/\delta$, and j, δ denote the imaginary unit and skin depth. The function $d(\boldsymbol{x})$ represents the distance from the surface of the conductor. Eq. (1) is intended to be assigned to the nodes or edges near the surface of the conductor. This is crucial for capturing the exponential change caused by the skin effect, which occurs at the surface of the conductor. We expect that the enrichment function extends the solution space for the tangential component of the electric field within the conductor.

In 2D problems, the XFE approximation of a scalar function $A(\boldsymbol{x})$ is expressed as follows:

$$\hat{A}(\boldsymbol{x}) = \sum_{i\in I} a_i N_i(\boldsymbol{x}) + \sum_{i\in E} N_i(\boldsymbol{x}) \sum_{j} \psi_j(\boldsymbol{x}) a_{ij} \tag{2}$$

where $N_i(\boldsymbol{x})$ denotes the ith node interpolation function, a_i, a_{ij} are unknowns at the ith node, $\psi_j(\boldsymbol{x})$ is the jth enrichment function that extends the solution space, and I, E are the set of nodes in the domain and enriched nodes, respectively. In the case of the enrichment function (1), we use only one enrichment function and thus one enrichment term.

Note that (2) is the formulation for 2D problems, but it should be added that XFEM is also applicable to 3D problems using the edge interpolation functions, which is common in eddy current analysis. The details are given in [6]. Also, it is worth noting that the low frequency limit of the XFE approximation corresponds to the CFE approximation, and the high frequency limit of it corresponds to the CFE approximation with SIBC. Therefore, we can use the approximation for a wide range of frequencies.

B. *Exact Boundary Representation*

While the use of a coarse mesh can significantly reduce the number of unknowns, it may result in a poor geometric approximation of the surface. To overcome this problem, we propose to combine XFEM and EBR. This approach encompasses various methods such as isoparametric FEM, p-FEM, NEFEM, and IGA. With this combination, eddy currents can be captured within the framework of XFEM while EBR is used to represent the exact shape of the surface in a coarse mesh.

The basic idea of EBR is to define an exact mapping from a reference domain onto a curved physical domain. Without loss of generality, we assume that triangles in the physical domain have one curved edge, as shown in Fig. 1. The mapping $\boldsymbol{\phi}(\xi,\eta)$ from the reference triangle K_t $(0 \le \xi, \eta, \xi+\eta \le 1)$ onto the curved triangle Ω_t can be defined by [7]

$$\boldsymbol{\phi}(\xi,\eta) = \frac{1-\xi-\eta}{1-\xi}\boldsymbol{C}(\xi) + \frac{\xi\eta}{1-\xi}\boldsymbol{x}_2 + \eta\boldsymbol{x}_3 \tag{4}$$

where $C(\xi)$ denotes a parametrization of the curved edge of Ω_t defined such that $C(0) = \boldsymbol{x}_1$, $C_1(1) = \boldsymbol{x}_2$, and $\boldsymbol{x}_k$, $k = 1,2,3$ are the vertices of Ω_t.

Once we obtain the exact mapping with the parametrization of the curved edge, the XFE approximation enhanced by EBR is defined by using the reference coordinates as follows:

$$\begin{aligned}\hat{A}(\xi,\eta) = \sum_{i\in I} a_i N_i(\xi,\eta) \\ + \sum_{i\in E} N_i(\xi,\eta) \sum_j \psi_j\big(\boldsymbol{\phi}(\xi,\eta)\big) a_{ij}\end{aligned} \tag{5}$$

where $N_i(\xi,\eta)$ is the interpolation function on K_t. The integration over the physical element can be computed as

$$\int_{\Omega_t} f(\boldsymbol{x})d\Omega = \int_{K_t} f(\xi,\eta)\left|J_\phi(\xi,\eta)\right| d\boldsymbol{\xi} \tag{6}$$

where $J_\phi(\xi,\eta)$ is the Jacobian matrix defined by using the exact mapping as follows:

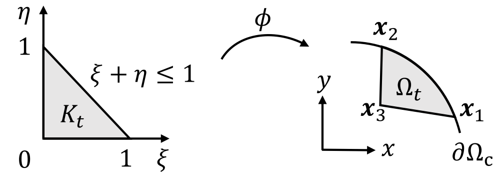

Fig. 1. Exact mapping from reference triangle to physical subdomain, which has a curved edge.

$$J_\phi(\xi,\eta) = \frac{\partial\boldsymbol{\phi}(\xi,\eta)}{\partial(\xi,\eta)}. \tag{7}$$

Because the enrichment function (1) and the exact mapping (4) are not polynomial functions, the integral in the weak formulation must be evaluated numerically using the Gaussian quadrature. Although the cost of the numerical quadrature is usually higher than the analytical formula, the total computation time would reduce because the time to solve the equation is longer than the time to assemble the FE matrix in large scale problems. As well as XFEM, the EBR method is not restricted to the 2D problems but can also be used in the 3D problems with both node and edge interpolation functions by constructing the exact mapping from the reference domain onto the curved physical domain.

C. *Variations of the enrichment functions*

In the case of the round conductor, we can consider other forms of the enrichment function that may improve the expression of the eddy currents. Considering the general solution of the 2D Helmholtz equation in the cylindrical coordinates, we obtain the following functions

$$\begin{aligned}\psi_{2m}(\boldsymbol{x}) &= J_m\big(kr(\boldsymbol{x})\big)\cos(m\theta), \\ \psi_{2m+1}(\boldsymbol{x}) &= J_m\big(kr(\boldsymbol{x})\big)\sin(m\theta), m = 0,1,2,\cdots\end{aligned} \tag{8}$$

where $J_m(x)$ denotes the mth order Bessel function of the first kind, $k = (1-j)/\delta$, and $r(\boldsymbol{x})$ is the distance from the center of the round conductor. In particular, $\psi_0(\boldsymbol{x})$ corresponds to the analytical solution of the skin effect under the time-harmonic uniform current density, and $\psi_2(\boldsymbol{x})$ and $\psi_3(\boldsymbol{x})$ correspond to that of the proximity effect under the time-harmonic uniform applied magnetic field.

At low frequencies, the use of these enrichment functions is expected to improve the accuracy of the eddy current analysis including the round conductor because the effect of the curvature on the solution is incorporated in (8). However, at high frequencies, the asymptotic forms of the Bessel functions are proportional to the exponential function, which renders the use of the high order Bessel functions unnecessary.

Based on our preliminary study, however, we did not observe any improvement in accuracy for the models we used, which means the exponential function works very well. Therefore, we refrain from comparing the Bessel functions with the exponential function in the subsequent analysis.

III. Numerical Result

In this section, we validate the proposed method using 2D problems, but it should be emphasized that the same effect can be achieved in 3D problems as well.

A. *Skin effect in round conductor*

First, we consider a round conductor of radius $a = 0.01$ [m], conductivity $\sigma = 5 \times 10^7$ [S/m], and relative permeability $\mu_r = 1$ to which the time-harmonic unit voltage is applied. The analysis domain Ω is bounded by Γ_D. The Cartesian coordinate system (x, y, z) is introduced as illustrated in Fig. 2 (a), and the z-component of the magnetic vector potential A_z is governed by

$$-\nabla \cdot \nu \nabla A_z + j\omega\sigma A_z = J_0, \qquad \text{in } \Omega \tag{9}$$
$$A_z = 0, \qquad E_0 = 1, \qquad \text{on } \Gamma_D \tag{10}$$

where $J_0 = \sigma E_0$ and $\nu = \mu^{-1}$.

The finite element discretization of the analysis domain is shown in Fig. 2 (b), where the exact geometry of the curved boundary Γ_D is treated in the proposed method. The nodes in gray elements were enriched in XFEM, and 15th-order Gaussian quadrature was used for the numerical quadrature to ensure the accuracy at the high frequencies. The numbers of degrees of freedom (DoFs) are 41 and 71 in CFEM and XFEM, respectively. We compared the solution with the analytical solution obtained by solving the equation in the cylindrical coordinate system (r, θ, z) given by:

$$A_z(r) = -\frac{1}{j\omega}\left(\frac{J_0(kr)}{J_0(ka)} - 1\right), \tag{11}$$
$$E_z(r) = \frac{J_0(kr)}{J_0(ka)}, \tag{12}$$

where $k = \sqrt{-j\omega\sigma\mu}$. The exact solutions satisfy $A_z(a) = 0$, $E_z(a) = 1$, on Γ_D. We also compared the proposed method with the SIBC approximation given by:

$$E_z(r) = \exp\left(-\gamma(a - r)\right), \tag{13}$$
$$H_\theta(r) = \sqrt{\frac{\sigma}{j\omega\mu}} \exp\left(-\gamma(a - r)\right) \tag{14}$$

where $\sqrt{j\omega\mu/\sigma}$ is the so-called surface impedance, which is the first order approximation.

The AC resistance and inductance were computed by CFEM and XFEM and compared with the analytical solution as shown in Fig. 3 and 4. The x-axis of the Figs is the normalized radius a/δ which is an indicator of the strength of the skin effect. We can see that the proposed combination of XFEM with EBR is the most accurate for a wide range of frequencies. From these figures, we can observe that

1. From Fig. 3, the results obtained from XFEM at the low frequency limit correspond to those of CFEM.
2. At high frequencies, the results obtained from CFEM are unreliable. In fact, the size of the mesh $h \approx 2.0$ [mm] is too large against the skin depth $\delta \approx 2.25$ [mm] at $a/\delta \approx 4.4$ regardless of the use of EBR.
3. In contrast, the results obtained from XFEM with and without EBR are accurate even at high frequencies. The difference between the results obtained from XFEM with and without EBR is caused by the geometric approximation, which can clearly be seen at the DC resistance.
4. From Fig. 3, we can see that the error of the SIBC approximation increases at low frequencies. It is because the relation $\delta \ll a$, which is one of the assumptions of SIBC, does not hold at low frequencies. Nevertheless, the DC resistance is obtained accurately because the electric field (13) becomes constant $E_z(r) \to 1$ at the stationary limit $\omega \to 0$.
5. From Fig. 4, the inductance obtained from the SIBC approximation diverges because the magnetic field (14) becomes infinite $H_\theta(r) \to \infty$ at the stationary limit $\omega \to 0$.
6. At high frequencies, the results obtained from XFEM with EBR correspond to those obtained from the SIBC approximation.

Therefore, XFEM enhanced by EBR is most favorable in the above respects compared to CFEM, XFEM without EBR, and SIBC approximation.

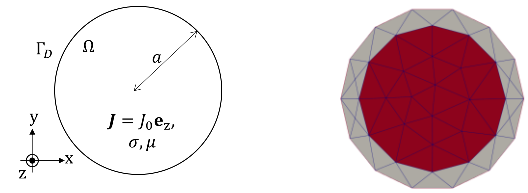

(a) Analysis domain (b) Coarse mesh

Fig. 2. (a) A round conductor and (b) mesh used in the analysis.

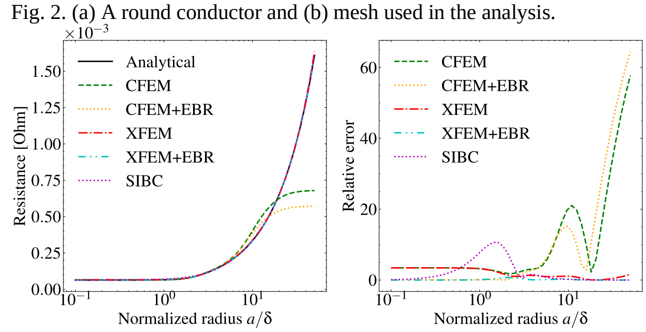

Fig. 3. AC resistance and its relative error obtained from CFEM and XFEM with and without EBR method are plotted against the frequency.

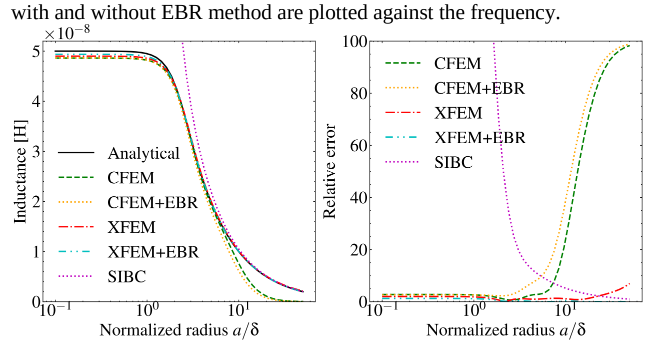

Fig. 4. Inductance and its relative error obtained from CFEM and XFEM with and without EBR method are plotted against the frequency.

B. *Skin and Proximity Effects between Multiple Conductors*

Next, we validate the proposed method for the 2-turn air core coil model shown in Fig. 5 (a). The radius, conductivity, and relative permeability of the conductor are the same value as those used in the previous section, and the unit current flows in each conductor. Skin and proximity effects occur between the coils, resulting in asymmetrically biased current density. Fig. 5 (b) shows the real part of the current density at 10^3 Hz. We can see the current density is asymmetric due to the proximity effect. The z-component of the magnetic vector potential A_z is governed by

$$-\nabla \cdot \nu \nabla \mathrm{A_z} + j\omega\sigma A_z + \frac{\partial \phi}{\partial z} = J_0, \qquad \text{in } \Omega \tag{15}$$

$$\int_{\Omega_C} \left(\sigma A_z + \frac{1}{j\omega} \frac{\partial \phi}{\partial z} \right) dS = 0, \tag{16}$$

$$\boldsymbol{B} \cdot \boldsymbol{n} = 0, \qquad \text{on } \Gamma_D, \tag{17}$$

$$\boldsymbol{H} \times \boldsymbol{n} = \boldsymbol{0}, \qquad \text{on } \Gamma_N, \tag{18}$$

where $\partial\phi/\partial z$ is an unknown value which is constant in the conductor region Ω_C. The corresponding boundaries Γ_D, Γ_N are illustrated in Fig. 5(a).

To assess the accuracy of the proposed method, we obtained a reference solution by solving the equation using a fine mesh that is sufficiently fine at high frequencies, as depicted in Fig. 6 (a). In the proposed method, the coarse mesh, illustrated in Fig. 6 (b), is used where the nodes in the light blue area were enriched in XFEM. The numbers of DoFs are 462 and 492 in CFEM and XFEM, respectively, whereas the number of DoFs in CFEM with reference mesh is 18,894.

The Joule losses and relative error compared to the reference solution were computed by CFEM and XFEM with and without EBR, as shown in Fig. 7. It can be observed that the proposed method exhibits the highest accuracy over a wide range of frequencies. In addition, it took 902 ms to obtain the reference solution while it took 124 ms to obtain the solution by XFEM with EBR at 10^3 Hz. The advantage of using EBR is that it requires almost the same amount of memory and computation time, yet improves accuracy.

IV. Conclusion

In this study, we validated the use of EBR in XFEM to enhance the geometric approximation. The numerical results demonstrated a significant reduction in errors due to the use of coarse mesh compared to the conventional FEM and XFEM approaches while keeping almost the same amount of memory consumption and computation time as XFEM without EBR. For future work, we will apply the proposed method to 3D eddy current problems. In addition, we plan to investigate the convergence property, time-domain analysis, and efficient numerical integration method.

Acknowledgment

This work was supported in part by the JSPS KAKENHI Grant Number 22K14237.

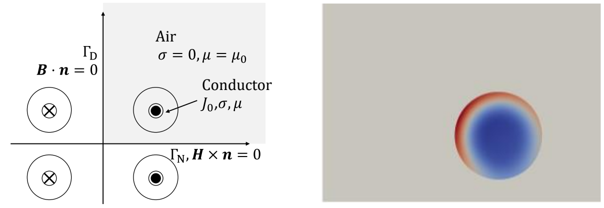

(a) Air core coil (b) Real part of J_z

Fig. 5. (a) 2-turn air core coil model where the skin and proximity effects occur in the conductor. Owing to the symmetry, the analysis domain is restricted to the upper half region. (b) The real part of the current density at 10^3 Hz ($a/\delta \approx 4.4$).

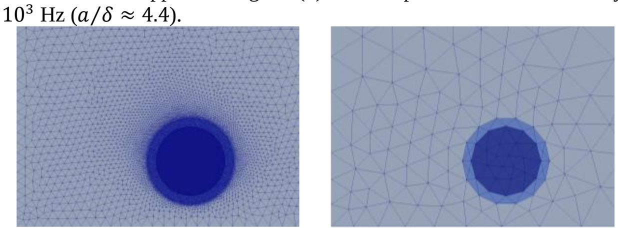

(a) Reference mesh (b) Coarse mesh

Fig. 6. (a) Fine mesh considering the skin depth and (b) coarse mesh not considering the skin depth at high frequency.

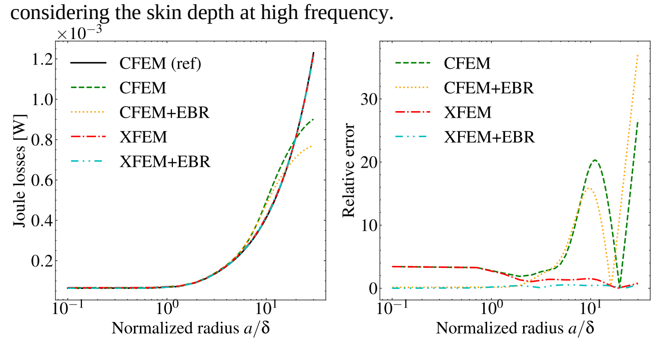

Fig. 7. Joule losses and its relative error to the reference solution plotted against the normalized radius.

References

[1] L. Krahenbuhl and D. Muller, “Thin Layers in Electrical Engineering Example of Shell Models in Analysing Eddy-Currents by Boundary and Finite Element Methods,” *IEEE Trans. Magn.*, vol. 29, no. 2, pp. 1450–1455, March 1993.

[2] J. Dong and L. D. Rienzo, "FEM and BEM Implementations of a High Order Surface Impedance Boundary Condition for Three-Dimensional Eddy Current Problems," *IEEE Access*, vol. 8, pp. 186496-186504, 2020.

[3] J. Gyselinck, P. Dular, N. Sadowski, P. Kuo-Peng and R. V. Sabariego, "Homogenization of Form-Wound Windings in Frequency and Time Domain Finite-Element Modeling of Electrical Machines," *IEEE Trans. Magn.*, vol. 46, no. 8, pp. 2852–2855, Aug. 2010.

[4] H. Igarashi, "Semi-Analytical Approach for Finite-Element Analysis of Multi-Turn Coil Considering Skin and Proximity Effects," *IEEE Trans. on Magns.*, vol. 53, no. 1, pp. 1-7, Jan. 2017.

[5] K. Hollaus, J. Schöberl and M. Schöbinger, "MSFEM and MOR to Minimize the Computational Costs of Nonlinear Eddy-Current Problems in Laminated Iron Cores," *IEEE Trans. Magn.*, vol. 56, no. 2, pp. 1–4, Feb. 2020.

[6] S. Hiruma, "Extended Finite Element Method for Calculation of Eddy Currents at High Frequencies," *IEEE Trans. Magn.*, vol. 59, no. 5, pp. 1-4, May 2023.

[7] R. Sevilla, S. Fernández-Méndez and A. Huerta, "Comparison of High-Order Curved Finite Elements," *International Journal for Numerical Methods in Engineering*, 87.8, 2011, pp. 719-734.

[8] Sevilla Cárdenas, Rubén, Sonia Fernández Méndez, and Antonio Huerta. "3D NURBs-Enhanced Finite Element Method." NMASE 07, 6th: 2007: Vall de Núria, 2009.

[9] A. Buffa, G. Sangalli and R. Vázquez, "Isogeometric Analysis in Electromagnetics: B-splines Approximation," *Computer Methods in Applied Mechanics and Engineering* 199.17-20, 2010, pp. 1143-1152.

[10] T. Belytschko, R. Gracie and G. Ventura, "A Review of Extended/Generalized Finite Element Methods for Material Modeling," *Model. Simul. Mater. Sci. Eng*., vol. 17, no. 4, pp. 043001, Apr. 2009.

[11] T. Strouboulis, I. Babuška and R. Hidajat, "The Generalized Finite Element Method for Helmholtz Equation: Theory Computation and Open Problems", *Comput. Methods Appl. Mech. Eng.*, vol. 195, no. 37, pp. 4711–4731, Jul. 2006.